

# Geospatial approach to analyse the impact of urban development on the urban heat island in Hisar city, Western Haryana, India

Dr. Surender Kumar Dr. Surender Kumar (✉ [spawar335@gmail.com](mailto:spawar335@gmail.com))

Dayanand College Hisar

Dr. Ripudaman Dr. Ripudaman

AISS Amity University, Noida

---

## Research Article

**Keywords:** Developing Countries, LST, NDVI, NDBI, South Asia, UHI, UTFVI

**Posted Date:** January 22nd, 2024

**DOI:** <https://doi.org/10.21203/rs.3.rs-3872191/v1>

**License:**  This work is licensed under a Creative Commons Attribution 4.0 International License. [Read Full License](#)

**Additional Declarations:** No competing interests reported.

---

# Abstract

The significant influence of urban development on land surface temperature (LST) was always evident. Here, a study of the temperature increases in Hisar city from 1991 to 2022 was conducted using Landsat data. The extent of thermal comfort in Hisar based on the urban thermal field variance index (UTFVI) was also evaluated. A land-use change map was used to calculate land-cover change, the NDVI was used to calculate vegetation coverage, and the NDBI was used to assess building cover. Over time, the UHI effect over Hisar city has significantly increased. It was found that built-up areas greatly affected the LST, especially at greater built-up densities. From 1991 to 2022, the minimum LST increased from 17.02°C to 37.40°C. Additionally, the highest temperature in 2022 increased to 47.24°C from 30.00°C in 1991. An inverse correlation was found between the LST and NDVI, which indicates that greenery has a debilitating effect on urban temperatures. However, the NDBI and LST, are positively correlated, indicating that urbanization intensifies the LST and causes the creation of urban heat islands (UHIs). The level of comfort for urban residents decreased during 1991–2022. Thus, urban heat management and sustainable city development require proper heat action plans.

## 1. Introduction

The environmental impacts of urban development are severe and complex [1–4]. In 2050, 68.4% of the global population will live in urban areas. Due to rapid urbanization, the number of people living in urban areas will increase to approximately 6.7 billion by 2050 [5]. A changing climate and diverse impacts on biodiversity are common in urban areas [6]. As one of the most significant urban environmental problems associated with urbanization, the urban heat island (UHI) effect is defined as the difference between the temperature in urban areas and that in surrounding rural areas [7–8]. Urbanization has substantially altered the composition of the near-surface atmosphere, as well as the balance of the Earth's surface radiation and energy [9–10]. Changes in building materials and colours, human-induced heat emissions [11], and climate change [12], all contribute to UHIs. A large increase in urbanization is expected in India as well, with urban dwellers accounting for 35% (493 million) of the population in 2021 and reaching 877 million by 2050; this would account for the majority of the urban area by that time [5–13]. Due to increasing urbanization, it is important to understand why environmental change occurs differently in rural and urban areas across India [14].

Land-use change can be observed and measured globally, regionally, and locally as a result of socioeconomic processes such as population growth, economic development, trade, and migration [15–17]. The land surface temperature has always been significantly affected by urban development and this effect can also be observed in small urban patches with population less than 10,000 [18]. Historically, Luke Howard was the first to present evidence that the air temperature in cities is higher than the air temperature in the countryside [19–20]; however, this idea was later validated [21–22]. In this context, land surface temperature (LST) is considered to be one of the key parameters [23]. Several studies have shown that industrialization, in addition to other anthropogenic factors, increase the LST around urban centre worldwide [17, 24–26]. In urban areas, there are higher temperatures than in the natural environments surrounding them; this phenomenon is known as the urban heat island [27]. Among the factors, solar insolation, plant life, extent of urbanisation, density of built-up areas, topography, meteorological aspects, urban geometry, anthropogenic heat and water content determine urban heat island intensity over a period of time [28–31]. LULC patterns that are naturally or anthropogenically changed can significantly increase surface and atmospheric temperatures compared with those in undeveloped areas [32–34].

The global urban population has significantly increased from 30% (751 million) in 1950 to 55% (4.2 billion) in 2018 and is expected to reach 60% (5.2 billion) by 2030 and 68% (6.7 billion) by 2050 [5]. Moreover, rapid urban growth is being witnessed in South Asia, Latin America and Sub-Saharan Africa [35–37]. Urban heat island studies in South Asian megacities such as Hyderabad, Chennai, Dhaka, Chattogram, Khulna, Kolkata, and Chennai have increased significantly in recent years, and major concerns have been raised about the potential impact of these islands on the developing world [38]. Over the last few decades, India has also experienced rapid urbanization, which is expected to continue in the future [39]. The Smart City Program for 100 Cities was recently announced by the Indian government and will result in rapid urban infrastructure and population growth as well, resulting in further extreme temperatures, additional public health problems, increased energy usage for cooling homes, and increased the intensity of urban heat islands [14, 40]. Hotter and more frequent climate swings have contributed to increased heat stress and mortality in India, and future heatwaves are likely to intensify further [14, 22].

By introducing geospatial techniques for urban heat island effect estimation, the spatiotemporal distribution of land surface temperature can be easily retrieved [41]. In the present era of space technology, various sensors including Advanced Space-borne Thermal Emission and Reflection (ASTER), National Oceanic and Atmospheric Administration-Advanced Very High-Resolution Radiometer (NOAA -AVHRR), Moderate Resolution Imaging Spectroradiometer (MODIS), and Landsat TM/ETM+, which have different spectral and spatial resolutions are available for urban heat island studies [29, 42–45]. According to existing studies urban heat islands have been found in urban areas worldwide, particularly in developing countries such as Delhi and Mumbai [46]; Chandigarh, India [47]; Ludhiana and Mansa in Punjab [48–49]; Narayanganj, Bangladesh [17]; Tianjin city, China [50]; Penang city, Malaysia [51]; and developed countries such as Braganca, Portugal [52]. Most urban heat island studies have focused on estimating land surface temperature. Several urban heat island indicators including the NDVI, NDBI, land use/landcover change [53] and percent impervious area [49], have been studied to estimate their impact on urban heat islands.

Findings of these studies suggest that cities and towns undergoing rapid urbanization should be explored for UHI investigations, and Hisar city represents a suitable case. Using proper land use management measures, such as analysing trends in land surface temperature and other relevant parameters can minimize land use change related risks arising from urban heat island effects [54]. It is known as the 'Steel City' of Haryana and is one of the most important cities in western Haryana. It has achieved excellent prominence in the urban development field over the past few decades. In Hisar city, commercial and industrial development is already underway, and the road network is improving. It is a potential industrial and commercial hub in western Haryana. In Hisar District, we study the spatiotemporal patterns and the evolution of the "thermal landscape" during rapid urbanization, as well as the potential drivers and high-risk areas.

To analyse these parameters, this study examined the changes in the coefficients of LULC, LST, NDBI, and NDVI in Hisar city during 1991, 2001, 2011 and 2022 to assess the urban heat island intensity. Urban planners and policymakers can use the findings of this study to plan a sustainable urban environment for Hisar and other cities in developing countries.

## 2. Materials and Methods

### 2.1 Study area

For the present research, the boundary of Hisar city was demarcated from Google Earth referencing the property listing map of Haryana [55]. Hisar city is situated in western Haryana in northwestern India. The longitudinal and latitudinal extents of the study area are  $75^{\circ} 40'14.425''$  E to  $75^{\circ} 52'15.298''$  E and  $29^{\circ} 06'3.177''$  N to  $29^{\circ} 12'9.617''$  N latitude. The study area covers an area of 109.31 square kilometres, as calculated by GIS software. It is located in the Great Plains of India. Because of its dry climate, Hisar city receive little rainfall.

The summers are very hot, and the winters are relatively cool. During the summer, temperatures can reach 40 to 46 degrees Celsius while they range from 1.5°C to 4°C during winter. The southwest monsoon season occurs between mid-June and mid-September. From October to June, the weather is almost dry while sometimes, western disturbances cause 10 to 15% of the rainfall during this period. From June to September, only 75 to 80% of the annual rainfall occurs in the study area. The city has good rail and road networks connecting it to its surrounding areas [56]. Figure 1 shows the location map of the study area.

## 2.2 Data procurement

To determine the land surface temperature characteristics, Landsat series data from Landsat 5, 7, and 9 for the month of March for the years 1991, 2001, 2011 and 2022 were processed from the USGS Earth Explorer (Table 1). Cloudy pixels are not present in all the downloaded satellite data. The software ArcGIS 10.2 was used to perform the relevant tasks for land surface temperature computation on all the images.

Table 1  
Details of the Landsat Satellite Data

Satellite/Sensor	Path/Row	Date	Pixel Cell Size
Landsat 5 / TM	147/40	05/03/1991	30
Landsat 7 / ETM+	147/40	08/03/2001	30
Landsat 5 / TM	147/40	12/03/2011	30
Landsat 9 / (OLI&TIRS)	147/40	18/03/2022	30

## 2.3 Procedure for Land Surface Temperature Calculations

Different methods (Fig. 2) were used for calculating the land surface temperature from thermal band 6 of Landsat 5 and 7, while the average of thermal bands 10 and 11 of Landsat 9 were used for land surface temperature calculations [57–58].

### 2.3.1 Conversion of Digital Number into Radiance and TOA

To convert Digital Numbers (DNs) into spectral radiance values, the equation below was used for thermal band 6 of Landsat 5 and 7 (Eq. 1) [57, 59]. The digital numbers of thermal bands 10 and 11 in the Landsat 9 data were converted into top-of-atmosphere reflectance (TOA) values (Eq. 2) [60].

$$L(\lambda) = \frac{(L_{MAX\lambda} - L_{MIN\lambda})}{(QCAL_{MAX} - QCAL_{MIN})} * (QCAL_{MAX} - QCAL_{MIN}) + L_{MIN\lambda}$$

For Landsat 5

$$L(\lambda) = \frac{(15.303 - 1.238)}{(255 - 1)} * (Band6 - 1) + 1.238$$

For Landsat 7

$$L(\lambda) = \frac{(17.040 - 0.000)}{(255 - 1)} * (Band6 - 1) + 0.000$$

(Here: L ( $\lambda$ )- is the radiance of Sensor; LMAX $\lambda$ - is the band 6 maximum radiance; and LMIN $\lambda$ - is the band 6 Minimum radiance; QCALMAX- quantize cell maximum value; QCALMIN-quantize cell minimum value- available in MTL file of Landsat 5 and 7)

for Landsat 9

$$L(\lambda) = M_L Q_{CAL} + A_L$$

2

$$L(\lambda) = 0.0003342 * Band10 + 0.1; L(\lambda) = 0.0003342 * Band11 + 0.1$$

(Here

L( $\lambda$ )- TOA spectral radiance; -Band specific multiplicative scaling factor; -Band specific additive factor; -Quantize and calibrated standard cell value- in MTL file)

## 2.3.2 Conversion to temperature

After converting the cell value to radiance and TOA, the land surface area was calculated by using Eq. (3).

$$T = \left( \frac{K2}{\ln \left( \frac{K1}{L} + 1 \right)} \right) - 273.15$$

3

For Landsat 5 For Landsat 7

$$T = \left( \frac{1260.56}{\ln \left( \frac{607.76}{L} + 1 \right)} \right) - 273.15 T = \left( \frac{1282.71}{\ln \left( \frac{666.09}{L} + 1 \right)} \right) - 273.15$$

For Landsat 9 (Band 10) For Landsat 9 (Band 11)

$$T = \left( \frac{1321.08}{\ln \left( \frac{774.89}{L} + 1 \right)} \right) - 273.15 T = \left( \frac{1201.14}{\ln \left( \frac{480.89}{L} + 1 \right)} \right) - 273.15$$

(Here: T-Effective at satellite temperature in Kelvin; K2-Calibration Constant 2; K1-Calibration Constant 1 (Available in MTL file); L-Spectral Radiance of Bands 6, 10, and 11)

After calculating the T of bands 10 and 11 of Landsat 9, the average value of both bands was calculated by the Cell Statistics Tool in Data Management Tools of ArcGIS software.

For Landsat 4 and 5, land surface temperature data were collected. However, for the Landsat 9 data, equations 3, [4](#) and 5 are used to calculate the land surface temperature:

$$LSE = 0.004 * Pv + 0.986$$

3

$$Pv = (NDVI - NDVImin / NDVImax - NDVImin)^2$$

4

$$Pv = (NDVI - (-0.00358388) / 0.500043 - (-0.00358388))^2$$

$$LST = \frac{BT}{1 + W * \left( \frac{BT}{p} \right) * \ln(e)}$$

5

$$LST = \frac{BT(Band10)}{1 + W(Band10) * \left( \frac{BT - Band10}{14380} \right) * \ln(LSE)}$$

## 2.4 NDVI calculation

Globally, normalized difference vegetation index (NDVI) is widely used to measure vegetation cover. Using satellite images of Landsat 5, 7 and 9, the index is calculated using differences in the near-infrared and red reflectance bands. An area that is densely vegetated has a positive NDVI value, while an area that is not vegetated has a negative value. It ranges from -1.0 to +1.0. the NDVI of Hisar city was calculated by Eq. 6 [61–62].

$$NDVI = \frac{NearInfraredBand - RedBand}{NearInfraredBand + RedBand}$$

6

(the band Combination for NDVIs of Landsat 5 and 7 are Band 4 = Infrared Band, and Band 3 = Red Band, while those for Landsat 9 are Band 5 = Infrared Band, and Band 4 = Red Band).

## 2.5 NDBI calculation

Building density is commonly measured using the normalized difference built-up index (NDBI). Shortwave infrared (SWIR) and near-infrared (NIR) reflections from built-up parts and bare soil were calculating based on Landsat 5, 7 and 9 satellite images. The NDBI value ranges from -1 to +1 and can be calculated by using Eq. 7 [61].

$$NDBI = \frac{SWIR - NearInfraredBand}{SWIR + NearInfraredBand}$$

7

(the band combination for NDVIs of Landsat 5 and 7 are Band 5 = SWIR Band, and Band 4 = Infrared Band; while those for Landsat 9 are Band 6 = SWIR Band, and Band 5 = Infrared Band).

## 2.6 Urban heat islands

In this research, using the average temperature during the day, the UHI effect was calculated. In urban areas, heat islands are caused by a higher average temperature in the surroundings areas. The LST was Calculated using Eq. 8 to compare the variations in UHIs from 1991 to 2022 [63].

$$UrbanHeatIsland = \frac{LandSurfaceTemperature - MeanLandSurfaceTemperature}{StandardDeviation}$$

8

## 2.7 Calculation of the Relative Land Surface Temperature

Different areas contribute differently to the thermal environment, so analyzing the relative value of land surface temperature (RLST) can help clarify this phenomenon [11, 64]. The RLST was calculated by using Eq. 9.

$$(RLST)_i^t = LST_i^t - Ave\ LST_i$$

(Here: t represents each of the ten years,  $LST_i^t$  represents the satellite sensed pixel's LST in year i, and  $Ave\ LST_i$  represents the average LST of the study area).

In this research, following a previous study [65], a high-temperature zone was defined as an area where the RLST exceeded two degrees Celsius ( $^{\circ}\text{C}$ ), this zone is called a regional heat island (RHI) in Hisar city, and the whole area was classified into five classes ( below 0, 0–3, 3–6, 6–9 and above 9).

## 2.8 Urban Thermal Field Variance Index

To describe the distribution of heat and health within an urban area, the UTFVI, the extent of urban thermal comfort, was calculated using Eq. 10. There are six different ecological evaluation indices for Hisar city based on thermal comfort level [66–67].

$$Urban Thermal Field Variance Index = \frac{LST_{Pixel} (\text{ }^{\circ}\text{C}) - \text{MeanLST}}{LST_{Pixel} (\text{ }^{\circ}\text{C})}$$

10

## 2.9 Unsupervised Image Classification

The study area was classified via unsupervised image classification via iso-cluster unsupervised classification with the help of LANDSAT series data [68]. The Hisar city has been classified into four categories as built-up area, barren land, vegetation and waterbody.

## 2.10 UHI trend and spatiotemporal distribution analysis

The traditional standard deviation ellipse (SDE) method is used to analyse the overall pattern and trend of LSTs in the study area. The standard deviation of the x and y coordinates was calculated using the average centre of the image, and the ellipse axis was determined based on the standard deviation by using equations 11 and 12 [65, 69].

$$(SDE) = \frac{\sqrt{\sum_{n=1}^t (x - meanX)^2}}{n}$$

11

$$(SDE) = \frac{\sqrt{\sum_{n=1}^t (y - meanY)^2}}{n}$$

12

Using time series, the SDE was used to represent landscape element distribution trends [65, 70] in the study area from 1991 to 2022.

## 2.11 Accuracy Assessment

It is necessary to use statistical techniques to test LULC classification for accuracy because this approach generates some errors. For this purpose, error matrix approaches are widely used. The kappa coefficient, user accuracy, producer accuracy, and overall accuracy cannot be assessed without an error matrix [71–72]. For ground truthing, 100 points were used to validate the output. Google Earth's historical data were used for accuracy assessment. The accuracy of the models was calculated by using equations 13–16 (Table 8).

$$\text{User Accuracy} = \frac{\text{Corrected pixel for each class}}{\text{Sum of classified pixel (Row Total)}} \times 100 \quad (13)$$

$$\text{Producer Accuracy} = \frac{\text{Corrected pixel for each classified category}}{\text{Reference pixel in that category (Column Total)}} \times 100 \quad (14)$$

$$\text{Overall Accuracy} = \frac{\text{Corrected classified pixel (Diagonal)}}{\text{total no of reference pixel}} \times 100 \quad (15)$$

$$\text{Kappa Coefficient} = \frac{\text{Total Sample} * \text{Total corrected sample} - \text{rowtotal and column total}}{(\text{multiplication of each row and column})} \times 100 \quad (16)$$

### 3 Results and Discussion

Based on the above methods and methodology, the acquired results are given and analysed below:

#### 3.1 LULC and LST

LST increases as a result of LULC change. The LULC in Hisar city changed significantly during the 31 years between 1991 and 2022 because of rapid urbanization. A 1991 study revealed that the areas under the categories "water bodies", "vegetation", "built-up areas" and "barren land" were 1.99 (1.8%), 61.73 (56.49%), 18.76 (17.17%), and 26.83 (24.54%) km<sup>2</sup> respectively. There were 1.75 (1.6%), 36.44 (33.33%), 41.72 (38.17%) and 29.40 (26.90%) km<sup>2</sup> under the "water body", "vegetation", "built-up area" and "barren land" classes, respectively, in 2001 (Fig. 6). "Water bodies", "vegetation", "built-up areas", and "barren land" accounted for 4.43 (4.05%), 34.90 (31.94%), 53.66 (49.09%), and 16.31 (14.92%) km<sup>2</sup> respectively, of the total area in 2011. Water bodies, vegetation, built-up areas, and barren land made up 3.36 (3.07%), 30.05 (27.49%), 64.14 (58.69%), and 11.76 (10.75%) km<sup>2</sup> of the total area in 2022, respectively. Only 18.76 km<sup>2</sup> of the city area was developed in 1991, but 64.14 km<sup>2</sup> has been developed in 2022, representing almost 58.69% of the total city area (Table 2). In this period of 31 years, the built-up area of Hisar city increased by nearly 41.51%, resulting in a 41.51% reduction in other land use. The area under the "vegetation" and "barren land" classes decreased by -46.75% from 1991 to 2020 and were converted to built-up areas and waterbodies (Fig. 4, Fig. 5; Table 3). As a result of these changes in LULC, the LST in Hisar city was significantly affected. The areas with higher temperatures can be observed in (Fig. 3), which shows mostly built-up areas. In total, approximately ten spots with the highest temperatures were taken from the LST of 2022 for ground truthing. Industrial, commercial, agricultural and residential establishments are most likely to be hot spots with the highest temperatures. During the period 1991–2022, the minimum LST reached 37.40°C, up from 17.02°C in 1991. Moreover, the highest temperature in 2022 has risen upward from 30.00°C in 1991 to 47.24°C (Table 4).

In the period 1991–2022, the lowest and highest temperatures in the city increased by almost 20.38°C and 17.24°C, respectively. Meteorological department officials said that maximum temperature rose five notches in Hisar city, and a hot summer occurred in Haryana, where Hisar has experienced 48°C temperatures on its hottest day in 2022 [73]. The maximum temperature in this study was 47.24°C in 2022, which matches the recorded data from meteorological departments. There is a 0.76°C variation here. It is evident from this that the study is relatively accurate and shows a reasonable degree of agreement. The relative values (RLSTs) from 1991 to 2022 are shown in Fig. 7. In Table 5, the minimum, maximum, and average LST values for 1991–2022 are shown. LSTs reached their highest point in 2022 (42.3°C), while they reached their lowest point in 1991 (23.51°C). For Hisar, the reported air temperature for the corresponding date was not significantly greater than 0.76 degrees Celsius, which confirms the accuracy of the LST data. The low resolution of Landsat images may limit the ability to compare different years due to limitations in image capture. A regional heat island (RHI) was defined as an area with an RLST > 3°C. There has been a significant increase in RHI connectivity since 1991, especially in the central, western, southeastern, and northeastern parts of Hisar. In the past few years, several isolated patches have gradually merged. This may be due to the rapid economic development and urbanization that has taken

place in Hisar, which has led to the expansion of built-up land. In Hisar's central, western, southeastern, and northeastern regions, the RHI increased from 1991 to 2022, but in its northwestern (lower land area) regions, the RHI decreased significantly, especially where the RLST was low.

Table 2  
Calculation of Temporal LULC area and (%) of Hisar

LULC	1991	2001	2011	2022				
Class	(Area)	(Area)	(Area)	(Area)				
	(km <sup>2</sup> )	(%)	(km <sup>2</sup> )	(%)	(km <sup>2</sup> )	(%)	(km <sup>2</sup> )	(%)
Water Body	1.99	1.80	1.75	1.6	4.43	4.05	3.36	3.07
Vegetation	61.73	56.49	36.44	33.33	34.90	31.94	30.05	27.49
Built-up Area	18.76	17.17	41.72	38.17	53.66	49.09	64.14	58.69
Barren Land	26.83	24.54	29.40	26.9	16.31	14.92	11.76	10.75

Table 3  
Temporal change in LULC from 1991 to 2022

Sr. No.	Class to Class Change	Area (km)	Sr. No.	Class to Class Change	Area (km)
1.	Barren Land - Built-up Area	19.75	9.	Vegetation - Built-up Area	29.86
2.	Barren Land - Vegetation	3.84	10.	Vegetation - Vegetation	22.22
3.	Barren Land - Barren Land	2.95	11.	Vegetation - Barren Land	7.38
4.	Barren Land - Water Body	0.29	12.	Vegetation - Water Body	2.20
5.	Water Body - Built-up Area	0.96	13.	Built-up Area - Built-up Area	13.55
6.	Water Body - Vegetation	0.37	14.	Built-up Area - Vegetation	3.58
7.	Water Body - Barren Land	0.10	15.	Built-up Area - Barren Land	1.32
8.	Water Body - Water Body	0.55	16	Built-up Area - Water Body	0.32

Table 4  
Area (km) under different temporal LST ranges in Hisar city

Year	LST Range						
	0–19.7	19.7–23.2	23.2–27.5	27.5–37.4	37.4–40.5	40.5–42.9	42.9–47.3
1991	20.18	62.12	25.36	1.65	-	-	-
2001	2.66	15.11	31.68	59.86	-	-	-
2011	-	16.64	57.61	35.06	-	-	-
2022	-	-	-	-	14.43	46.90	47.24

Table 5  
Statistics of Temporal LST of Hisar

Years	LST			
	Minimum	Maximum	Mean	Std. Deviation
1991	17.02	30.00	23.51	± 1.98
2001	18.15	36.38	27.26	± 3.20
2011	19.72	34.86	27.29	± 2.50
2022	37.40	47.2	42.3	± 1.43

The RHI of the standard deviation ellipse (SDE) results are presented in Fig. 8. In 1991 and 2022, the SDE ranges were mostly located in the central region and gradually shifted to the southwest, southeastern, north-eastern, and eastern regions. Furthermore, Table 6 demonstrates a decrease in rotation from 73.20 in 1991 to 69.26 in 2022, indicating a change in the spatial pattern of RHI from the centre to the east, west, and south with rapid urbanization in Hisar.

Table 6  
Temporal analysis of SDEs

Years	Minor Axis (km)	Major Axis (km)	SD_X	SD_Y	Rotation
1991	18.2	78.45	4.21	7.58	73.20
2001	17.1	79.23	4.35	8.21	71.24
2011	18.4	82.32	4.22	7.91	70.36
2022	17.3	82.56	4.33	6.84	69.26

### 3.2 Correlation between the NDBI and NDVI and between the LST

The LST of any surface area is strongly correlated with the NDVI and NDBI. The vegetation cover is greatest and the LST is lowest. The NDVI values ranged from (-0.3125 to 0.7183), which indicated that most of the area had more vegetation cover than did a built-up area, water body, or barren land (Fig. 9).

It is evident that there was an increase in "built-up areas" and a decrease in vegetated areas in 2001, judging by the NDVI values ranging from -0.5 to 0.4767 and negative values increasing over this time period. In 2011, the NDVI values ranged from (-0.5 to 0.4767) and the decreases were more pronounced than those in 2001's decreases, indicating that urban areas have grown more while vegetated areas have decreased more. Over 70% of the area has negative NDVI values in 2022, with 58.69% of the land under the built-up category. Figure 4, shows that most of the areas in the "vegetation" and "barren land" classes from 1991 to 2022 were converted into the "built-up" class. A simple linear regression model demonstrated a significant relationship between LST, and NDVI, and between LST and the NDBI (Fig. 10; Fig. 11). According to this relationship, the change in land use contributes to rising temperatures. The NDVI and NDBI variables were selected as independent variables for a simple linear regression model. When the vegetation density is high, the temperature decreases, while when the vegetation density is low, it increases (Fig. 9). As shown in Fig. 9, the NDVI exhibited an inverse relationship with

the LST with  $R^2$  values of 0.50, 0.38, 0.20 and 0.31 for 1991, 2001, 2011 and 2022. On the other hand, the NDBI and LST are strongly correlated, as indicated by the  $R^2$  values for 1991 to 2022 respectively (Fig. 10). There is a clear relationship between the built-up area and temperature, such that the higher the area is, the greater the temperature. The LST and NDVI have a negative correlation, which suggests that green space can reduce UHIs.

### 3.3 Urban heat island (UHI), comfort level of urban thermal load(CLUT) and UTFVI

Based on the results, the UHI effect increases in all directions from the inward to the outward direction of the city. There was a notable increase in UHIs from 1991 to 2022 in parts of the city that had built-up and lost vegetation, particularly in the southwestern, central, southern, and southeastern areas of Hisar city. The results showed that the temperature increased from 20.18°C in 1991 to 47.24°C in 2022. The UHI effect has increased over the past 31 years (Fig. 12). Based on these results, the maximum UHI over Hisar city were 28°C in 1991, 30°C in 2001, 37°C in 2011, and 47°C in 2022. The minimum UHI value (18°C) occurred in 1991, whereas the minimum UHI value (37°C) increased in 2022. To determine the urban thermal comfort level and discomfort zone for human life, the UTFVI is classified into six classes based on the UHI effect. As a result, 57.01 km<sup>2</sup> (52.15%), 65.46 km<sup>2</sup> (59.87%), 59.01 km<sup>2</sup> (53.94%), and 39.72 km<sup>2</sup> (36.3%) have excellent-normal comfort for human life while 51.23 km<sup>2</sup> (47.35%), 43.85 km<sup>2</sup> (40.13%), 50.30 km<sup>2</sup> (46.06%) and 69.59 km<sup>2</sup> (63.7%) have the strongest-strongest UHIs in 1991, 2001, 2011 and 2022, respectively categorized as the worst-worst zones for human life due to heat and warming (Table 7). The ecological status of the Hushi city was determined by the UTFVI and UHI values.

Figure 12: UHI and CLUT maps (A, A1; B1, B2; C1, C2; C1,C2 for 1991;2001;2011;2022)

Table 7  
Measurement of UHI and CLUT based on the UTFVI

UTFVI	Phenomenon of UHI	Comfort level of urban thermal (CLUT)	HUI/CLUT		HUI/CLUT		HUI/CLUT		HUI/CLUT	
			Area (1991)		Area (2001)		Area (2011)		Area (2022)	
			sq. km	(%)						
< 0	None	Excellent	11.96	10.95	19.63	17.95	13.85	12.67	6.04	5.5
0–0.005	Weak	Good	24.34	22.26	16.97	15.52	35.52	32.45	18.82	17.21
0.005–0.01	Middle	Normal	20.71	18.94	28.86	26.4	9.64	8.82	14.86	13.59
0.01–0.015	Strong	Bad	34.57	31.62	19.79	18.1	23.28	21.34	38.23	34.91
0.015–0.02	Stronger	Worse	13.20	12.07	8.73	7.98	18.18	16.63	10.58	9.67
> 0.02	Strongest	Worst	4.53	4.16	15.33	14.05	8.84	8.09	20.78	19.12

Table 8  
Accuracy assessment analysis

LULC	User Accuracy (%)				Producer Accuracy (%)			
	Class	1991	2001	2011	2022	1991	2001	2011
Water Body	89.0	90.0	92.1	95.0	86.6	93.5	90.2	95.0
Vegetation	88.0	90.0	93.0	95.0	84.1	91.2	93.1	95.0
Built-up Area	89.0	90.0	94.0	95.0	86.0	93.1	95.0	95.0
Barren Land	83.0	90.0	90.0	95.0	80.2	86.5	90.3	95.0
Overall Accuracy (%)				Kappa Coefficient (%)				
	1991	2001	2011	2022	1991	2001	2011	2022
Water Body	86.6	93.0	92.0	95.0	80.0	80.8	81.6	84.1
Vegetation	85.0	92.0	92.0	95.0	80.0	81.0	81.6	84.1
Built-up Area	86.2	93.0	92.0	95.0	80.0	81.0	81.6	84.1
Barren Land	82.0	86.0	92.0	95.0	80.0	80.8	81.6	84.1

## Discussion

According to the present study, there were clear correlation between UHI, biodiversity loss, and ecosystem degradation and LULC around cities. Impacts, such as the decline in vegetation coverage, the increase in minimum and maximum temperatures, which directly affect the urban thermal environment, have been identified. Biodiversity and natural ecosystems are adversely affected by rapid urbanization [74]. With the exponential growth of Hisar city's population, and with its massive industrial and commercial expansion, its land use has changed significantly. Prior to 1991, the land in Hisar city was mainly agricultural, barren land, and covered with vegetation and these areas were converted into industries and residential areas after 1991. Its rapid population growth coupled with residential industrial, and commercial expansion had major impact on its solar radiance and longwave radiation (LST). In the built-up areas, the temperature increased significantly between 1991 and 2022. There are several densely developed commercial and residential areas in the city, including the Jindal industrial area, automobile market, Mil Gate, Azad Nagar, bus stand, airport, court complex, and old Hisar area. Due to the low amount of vegetation and water bodies in this area, heat islands and higher LST values are now predominant here. The above places had the highest heat island spots, while agricultural university and city boundary had the lowest LST values. As this study revealed, the average temperature in Hisar city increased with increasing minimum temperatures.

LULC types and LSTs have been found to be directly related to UHI trends. The NDVI and LST in the study area were inversely related for all types of LULC. Compared to other areas, industrial, residential and commercial areas had the highest LSTs and the greater influence on the NDVI. Increasing vegetation cover in Hisar city is therefore the best way to reduce temperature. The study area's urban heat characteristics can be improved by increasing vegetation cover in built-up areas, particularly industrial, commercial and nearby residential areas. Based on the NDVI analysis of 1991, the city in 2022 could not be accurately represented, because there was a decrease in

vegetation in most of the locations. As a result of infrastructure construction projects encroaching into existing vegetation, trees are being cut down, contributing to a higher LST. In addition, this results in pollution that worsens Hisar's situation. As an industrial city, Hisar should prioritize low carbon emissions. It is important for local governments to take precautions to encourage industries to reduce emissions and implement green initiatives. Youths in Hisar city should be made aware of extreme heat risks through a pilot campaign. Through the creation of short videos with messages in the local language, the campaign focused on the risks of heat and the ways to reduce them. Youths and policymakers were able to engage through this platform [75]. As a means of raising awareness, local governments could take this type of initiative. It is important for local governments to promote early warning or robust forecast systems to reduce the effects of LSTs and UHIs, even though their resources and budget are limited. They can also create spray parks for cooling, urban forests, cooling centres for communities, elimination of smoke-emitting vehicles, and paint roofs to cool them. A heat action plan should also be prepared by the national government and the local government because different regions have different drivers and intensities of heat. By doing so, we will be able to identify city hotspots and take action to reduce the effects of UHIs.

## Conclusion

Almost every country in the world has been affected by urban heat islands for more than a century. As urbanization increases in developing countries, UHI assessment is becoming an essential tool for urban growth management. Urbanization and environmental change are directly responsible for increase in surface temperatures in urban areas. A landscape of concrete and asphalt replaces vegetation and water bodies, while agricultural lands are converted into barren lands, which absorb solar radiation rather than reflecting it. This increases both the surface and ambient temperatures.

By using geospatial techniques, this study was conducted to determine the urban heat island effect in Hisar city from 1991 to 2022. Landsat and ETM data were used to assess LULC, NDVI, and NDBI and how they impact LST. There has been a significant increase in the overall surface temperature of the city as a result of the built-up area, with the bus stop, Mile Gate, airport, court complex, old city, railway station, Jindal Industrial Park, etc., of Hisar city experiencing the greatest increase in LST. Compared to those in 1991, 2001, and 2011, the 2022 temperature was lower in terms of vegetation and agriculture but was consistently higher than in 1991, 2001, and 2011. The presence of vegetation and water bodies appeared to be significant factors in lowering the surface temperature. During the past 31 years, the vegetation cover has decreased significantly, resulting in increased temperatures. In some areas, the restoration of waterbodies and the planting of trees have helped to reduce surface temperatures in addition to the overall delineation of agricultural land, water bodies and habitats. Despite of the low resolution of satellite images such as those from Landsat 5, 7 and 9, the analyses of LULC change, NDVI, NDBI, and LST are not precise at the microlevel, however, the macrolevel results can be very useful for urban and environmental planners to formulate policies and strategies. It is necessary to obtain satellite images with higher resolution and ground truthing to make more accurate assessments at the microscopic level. This study has limitations due to the lack of cloud-free data, difficulties in collecting humidity data, and the absence of weather data. The findings of this study will be useful to other researchers, Hisar city, and local authorities for taking steps to reduce urban heat island effects and LSTs in Hisar.

## Declarations

# Conflicts of Interest

The authors declare no conflicts of interest.

## Funding

The research was not funded by any funding agency.

## Author Contribution

Dr. Surender Kumar wrote and prepared the results. Dr. Ripudaman reviewed the manuscript.

## Acknowledgement

The authors are pleased to thank the USGS for providing free and accessible satellite images and the director of urban local bodies, Haryana, for demarcating the boundaries of the study area. The anonymous reviewers' comments and advice are gratefully acknowledged.

## References

1. Seto K, Guneralp B, Hutyra L (2012) Global forecasts of urban expansion to 2030 and direct impacts on biodiversity and carbon pools. *Proceedings Of the National Academy of Sciences*. 109(40). 16083–16088. 10.1073/pnas.1211658109
2. Mishra V, Ganguly A, Nijssen B, Lettenmaier D (2015) Changes in observed climate extremes in global urban areas. *Environ Res Lett* 10(2):024005. 10.1088/1748-9326/10/2/024005
3. Singh R (ed) (2021) Re-envisioning Remote Sensing Applications: Perspectives from Developing countries, 1st edn. CRC Press, Taylor & Francis Group. <https://doi.org/10.1201/9781003049210>
4. Garcia DH, Diaz J, A (2022) Modeling the Surface Urban Heat Island (SUHI) to study of its relationship with variations in the thermal field and with the indices of land use in the metropolitan area of Granada (Spain). *Sustainable Cities and Society* 87:104166. <https://doi.org/10.1016/j.scs.2022.104166>
5. UN-Habitat (2022) World Cities Report 2022: Envisaging the Future of Cities. United Nations Human Settlements Programme, UN-Habitat, Nairobi
6. Grimm N, Faeth S, Golubiewski N, Redman C, Wu J, Bai X, Briggs J (2008) Global Change and the Ecology of Cities. *Science* 319(5864):756–760. 10.1126/science.1150195
7. Zhao L, Lee X, Smith RB, Oleson K (2019) Strong contributions of local background climate to urban heat islands. *Nature* 511:216–219
8. Oke TR (2002) Boundary layer climates. Routledge, London and New York
9. Foley JA, DeFries R, Asner GP, Barford C, Bonan G, Carpenter SR et al (2005) Global consequences of land use. *Science* 309:570–574
10. Yu Z, Yao Y, Yang G, Wang X, Vejre H (2019) Spatiotemporal patterns and characteristics of remotely sensed region heat islands during the rapid urbanization (1995–2015) of Southern China. *Sci Total Environ*

- 674:242–254. 10.1016/j.scitotenv.2019.04.088
11. Fan H, Yu Z, Yang G, Liu TY, Liu TY, Hung CH et al (2019) How to cool hot-humid (Asian) cities with urban trees? An optimal landscape size perspective. *Agric For Meteorol* 265:338–348
  12. Chapman S, Watson JEM, Salazar A, Thatcher M, McAlpine CA (2017) The impact of urbanization and climate change on urban temperatures: a systematic review. *Landscape Ecol* 32:1921–1935
  13. United Nations (2018) *World Urbanization Prospects 2018*. United Nations, New York
  14. Kumar R, Mishra V, Buzan J, Kumar R, Shindell D, Huber M (2017) Dominant control of agriculture and irrigation on urban Heat Island in India. *Sci Rep* 7(1):14054. <https://doi.org/10.1038/s41598-017-14213-2>
  15. Goklany IM (1996) Factors affecting environment impacts: the effect of technology on long-term trends. *Ambio* 25(8):497–503. <http://www.jstor.org/stable/4313529>
  16. IPCC (2007) *The fourth assessment report*. Geneva, Switzerland
  17. Rashid N, Alam JAMM, Chowdhury MA, Islam SLU (2022) Impact of landuse change and urbanization on urban heat island effect in Narayanganj city, Bangladesh: A remote sensing-based estimation. *Environmental Challenges*. 8. 100571. <https://doi.org/10.1016/j.envc.2022.100571>
  18. Karl TR, Diaz HF, Kukla G (1998) Urbanization: its detection and effect in the United States climate record. *J Clim* 1(11):1099–1123. [https://doi.org/10.1175/1520-0442\(1988\)001<1099:UIDAEI>2.0.CO;2](https://doi.org/10.1175/1520-0442(1988)001<1099:UIDAEI>2.0.CO;2)
  19. Howard L (1833) *The climate of London: deduced from meteorological observation made in the metropolis*, 1, London
  20. Oke TR (1982) The energetic basis of the urban heat island. *Q J R Meteorol Soc* 108(455):1–24. <http://doi.org/10.1002/qj.49710845502>
  21. Weng Q (2001) A remote sensing and GIS evolution of urban expansion and its impact on surface temperature in the Zhujiang Delta, China. *Int J Remote Sens* 22(10):1999–2014. <https://doi.org/10.1080/713860788>
  22. Murari KK, Ghosh S, Patwardhan A, Daly E, Salvi K (2015) Intensification of future severe heat waves in India and their effect on heat stress and mortality. *Reg Environ Chang* 15(4):569–579. <https://doi.org/10.1007/s10113-014-0660-6>
  23. Li Z, Tang B, Wu H, Ren H, Yan G, Wan Z, Trigo IF, Sobrino JA et al (2013) Satellite-derived land surface temperature: Current status and perspectives. *Remote Sens Environ* 131:14–37. <https://doi.org/10.1016/j.rse.2012.12.008>. Z.-L
  24. Yao R, Wang L, Huang X, Sun L, Chen R, Wu X, Zhang W, Niu Z (2021) A robust method for filling the gaps in MODIS and VIIRS land surface temperature data. *IEEE Trans Geosci Remote Sens* 59(12):10738–10752. <https://doi.org/10.1109/TGRS.2021.3053284>
  25. Ayanlade A (2016) Seasonality in the daytime and night-time intensity of land surface temperature in a tropical city area. *Sci Total Environ* 557–558. <https://doi.org/10.1016/j.scitotenv.2016.03.027>
  26. Bai Y, Yao L, Wei T, Tian F, Jin DY, Chen L, Wang M (2020) Presumed asymptomatic carrier transmission of Covid-19. *JAMA* 323(14):1406–1407. <https://doi.org/10.1001/jama.2020.2565>
  27. Voogt JA, Oke TR (2003) Thermal remote sensing of urban climates. *Remote Sens Environ* 86(3):370–384. [https://doi.org/10.1016/S0034-4257\(03\)00079-8](https://doi.org/10.1016/S0034-4257(03)00079-8)
  28. Oke TR (1987) *Boundary layer climate* (2nd ed), X(L) p. 435. Routledge. Chen, H.M Zhao, P. X. Li, J. Yin, Remote sensing imaged-based analysis of the relationship between urban heat island and land use/cover

- changes. *Remote Sensing Environment*. 104 (2006). 133–146. 10.1016/j.rse.2005.11.016
29. Chen XL, Zhao HM, Li PX, Yin ZY (2006) Remote sensing image-based analysis of the relationship between urban heat island and land use/cover changes. *Remote Sens Environ* 104(2):133–146.  
<https://doi.org/10.1016/j.rse.2005.11.016>
30. Taha H (1997) Urban climates and heat islands: Albedo, evapotranspiration, and anthropogenic heat. *Energy Build* 25(2):99–103. [https://doi.org/10.1016/S0378-7788\(96\)00999-1](https://doi.org/10.1016/S0378-7788(96)00999-1)
31. Xiong Y, Zhang J, Yan Y, Sun S, Xu X, Higueras E (2022) Effect of the spatial form of Jiangnan traditional villages on microclimate and human comfort. *Sustainable Cities and Society* 87:104136.  
<https://doi.org/10.1016/j.scs.2022.104136>
32. Clinton N, Gong P (2013) MODIS detected surface urban heat islands and sinks; Global locations and control. *Remote Sens Environ* 134:294–304. <https://doi.org/10.1016/j.rse.2013.03.008>
33. Kalnay E, Cai M (2003) *Impact of urbanization and land use change on climate*. 423. 528–532
34. Sultana S, Satyanarayana ANV (2020) Assessment of Urbanisation and urban heat island intensities using Landsat imageries during 2000–2018 over a subtropical Indian city. *Sustainable Cities and Society*. 52.  
<https://doi.org/10.1016/j.scs.2019.101846>
35. Hong C, Burney JA, Pongratz J, Nabel JEMS, Mueller ND, Jackson RB, Davis SJ (2021) Global and regional drivers of land use emissions in 1961–2017. *Nature* 589(7843):554–561. <https://doi.org/10.1038/s41586-020-03138-y>
36. Kotharkar R, Ramesh A, Bagade A (2018) Urban Heat Island studies in South Asia: A critical review. *Urban Climate*. 24. 1011–1026. Retrieved from: <https://doi.org/10.1016/j.uclim.2017.12.006>
37. Kumar S, Singh R (2021) Geospatial Applications in Land Use/Land Cover Change Detection for Sustainable Regional Development: The Case of Central Haryana, India. *Geomatics and Environmental Engineering*, 15(3): 81–98. Retrieved from: <https://doi.org/10.7494/geom.2021.15.3.81>
38. Chaudhuri G, Mishra NB (2016) Spatio-temporal dynamics of land cover and land surface temperature in Ganges-Brahmaputra Delta: A comparative analysis between India and Bangladesh. *Appl Geogr* 68:68–83.  
<https://doi.org/10.1016/j.apgeog.2016.01.002>
39. Dholkia HH, Mishra V, Garg A (2015) Predicted increase in heat mortality under climate change in urban India. *Indian Inst Manag Ahmedabad Work Pap* 2015–5–2:1–31
40. Mazdiyasni O, AghaKouchak A, Davis SJ, Madadgar S, Mehran A, Ragno E, Sadegh M, Sengupta A, Ghosh S, Dhanya CT, Niknejad M (2017) Increasing probability of mortality during Indian Heat waves. *Sci Adv* 3(6):e1700066. <https://doi.org/10.1126/sciadv.1700066>
41. Imhoff ML, Zhang P, Wolfe RE, Bounoua L (2010) Remote sensing of the urban heat island effect across biomes in the continental USA. *Remote Sens Environ* 114(3):504–513.  
<https://doi.org/10.1016/j.rse.2009.10.008>
42. Roth M, Oke TR, Emery WJ (1989) Satellite-derived urban heat islands from three coastal cities 37 and the utilization of such data in urban climatology. *Int J Remote Sens* 10(11):1699–1720.  
<https://doi.org/10.1080/01431168908904002>
43. Liu L, Zhang Y (2011) Urban heat island analysis using the Landsat TM data and ASTER data: A case study in Hong Kong. *Remote Sens* 3(7):1535–1552. <http://doi.org/10.3390/rs3071535>

44. Pandey P, Kumar D, Prakash A, Masih J, Singh M, Kumar S, Jain VK, Kumar K (2012) A study of urban heat island and its association with particulate matter during winter months over Delhi. *Sci Total Environ* 414:494–507. <https://doi.org/10.1016/j.scitotenv.2011.10.043>
45. Singh R (ed) (2022) Re-envisioning Advances in Remote Sensing: Urbanization, Disasters and Planning, 1st edn. CRC Press, Taylor & Francis Group. <https://doi.org/10.1201/9781003224624>
46. Grover A, Singh RB (2015) Analysis of urban heat island (UHI) in relation to normalized difference vegetation index (NDVI): A comparative study of Delhi and Mumbai. *Environments* 2(4):125–138. <https://doi.org/10.3390/environments2020125>
47. Mathew A, Khandelwal S, Kaul N (2016) Spatial and Temporal Variations of Urban Heat Island Effect and the effect of Percentage Impervious Surface Area and Elevation on Land Surface temperature: Study of Chandigarh City, India. *Sustainable Cities and Society* 26:264–277. <http://doi.org/10.1016/j.scs.2016.06.018>
48. Singh R, Kalota D (2019) Urban Sprawl and Its Impact on Generation of Urban Heat Island: A Case Study of Ludhiana City. *J Indian Soc Remote Sens* 47:1567–1576. <https://doi.org/10.1007/s12524-019-00994-8>
49. Kaur R, Pandey P (2020) Monitoring and spatiotemporal analysis of UHI effect for Mansa district of Punjab, India. *Adv Environ Res* 9(1):19–39. <https://doi.org/10.12989/aer.2020.9.1.019>
50. Ullah N, Siddique MA, Ding M, Grigoryan S, Zhang T, Hu Y (2022) Spatiotemporal impact of urbanization on urban heat island and urban thermal field variance index of Tianjin City, China. *Buildings* 12(4):399. <https://doi.org/10.3390/buildings12040399>
51. Zulayadini A et al (2022) Assessing the impacts of vegetation cover loss on surface temperature, urban heat island and carbon emission in Penang city. *Malaysia Building and Environment* 222 109335:1–19. <https://doi.org/10.1016/j.buildenv.2022.109335>
52. Almeida C, Rd, Furst L, Gonçalves A, Teodoro AC (2022) Remote sensing image-based analysis of the urban heat island effect in Bragança. *Portugal Environ* 9(8):98. <https://doi.org/10.3390/environments9080098>
53. Gallo KP, McNab AL, Karl TR, Brown JF, Hood JJ, Tarpley JD (1993) The use of a vegetation index for assessment of the urban heat island effect. *Int J Remote Sens* 14(11):2223–2230. <https://doi.org/10.1080/01431169308954031>
54. Noszczyk T, Rutkowska A, J., Hernik (2020) Exploring the land use change in Eastern Poland: Statistical-based modelling. *Hum Ecol Risk Assess Int J* 26(1):255–282. <https://doi.org/10.1080/10807039.2018.1506254>
55. Directorate of Urban Local Bodies. <https://pmsharyana.com/property/listing>. Haryana, India
56. Kumar A, Hooda RS, Bhatiya S (2016) Groundwater quality assessment for drinking purpose in Hisar city, Haryana. International Journal of Engineering Research and Technology (IJERT). *RACEE-2015 conference proceeding*. pp. 1–6
57. Sekertekin A, Bonafoni S (2020) Land surface temperature retrieval from landsat 5, 7, and 8 over rural area: Assessment of different retrieval algorithms and emissivity models and toolbox implementation. *Remote Sens* 12(2):294. <https://doi.org/10.3390/rs12020294>
58. Athick ASM, Shankar K, Naqvi HR (2019) Data on time series analysis of land surface temperature variation in response to vegetation indices in twelve Wereda of Ethiopia using mono window, split window algorithm and spectral radiance model. *Data in Brief* 27:104773. <https://doi.org/10.1016/j.dib.2019.104773>

59. Yue W, Xu J, Tan W, Xu L (2007) The relationship between land surface temperature and NDVI with remote sensing: Application to Shanghai Landsat 7 ETM + data. *Int J Remote Sens* 28(15):3205–3226. <https://doi.org/10.1080/01431160500306906>
60. Mancino G, Ferrara A, Padula A, Nolè A (2020) Cross-comparison between landsat 8 (OLI) and landsat 7 (ETM+) derived vegetation indices in a Mediterranean environment. *Remote Sens* 12(2):291. <https://doi.org/10.3390/rs12020291>
61. Kshetri T (2018) Ndvi, ndbi and ndwi calculation using landsat 7, 8. *Researchgate. Net* 327971920
62. Epiphanio JN, Huete AR (1995) Dependence of NDVI and SAVI on sun/sensor geometry and its effect on fAPAR relationship in alfalfa. *Remote Sens Environ* 51(3):351–360. [https://doi.org/10.1016/0034-4257\(94\)00110-9](https://doi.org/10.1016/0034-4257(94)00110-9)
63. Abutaleb K et al (2015) Assessment of urban heat island using remotely sensed imagery over Greater Cairo, Egypt. *Adv Remote Sens* 04(1):35–47. <https://doi.org/10.4236/ars.2015.41004>
64. Sun R, Chen L (2017) Effects of green space dynamics on urban heat islands: Mitigation and diversification. *Ecosyst Serv* 23:38–46
65. Yu Z, Yao Y, Yang G et al (2019) Spatiotemporal patterns and characteristics of remotely sensed regional heat islands during the rapid urbanization (1995–2015) of Southern China. *Sci Total Environ.* <https://doi.org/10.1016/j.scitotenv.2019.04.088>
66. Ahmed S (2018) Assessment of urban heat islands and impact of climate change on socioeconomic over Suez Governorate using remote sensing and GIS techniques. *Egypt J Remote Sens Space Sci* 21(1):15–25. <https://doi.org/10.1016/j.ejrs.2017.08.001>
67. Abir FA, Ahmmmed S, Sarker SH, Fahim AU (2021) Thermal and ecological assessment based on land surface temperature and quantifying multivariate controlling factors in Bogura. *Bangladesh Heliyon* 7(9):e08012. <https://doi.org/10.1016/j.heliyon.-2021.208012>
68. Nijhawan R, Srivastava I, Shukla P (2017) Land cover classification using super-vised and unsupervised learning techniques International Conference on Computational Intelligence in Data Science (ICCIDDS). 2017. 1–6. <https://doi.org/10.1109/ICCIDDS.2017.8272630>
69. Lefever DW (1926) Measuring Geographic Concentration by Means of the Standard Deviational Ellipse. *Am J Sociol* 32:88–94
70. Peng J, Chen S, Lü H, Liu Y, Wu J (2016) Spatiotemporal patterns of remotely sensed PM 2.5, concentration in China from 1999 to 2011. *Remote Sens Environ* 174:109–121
71. Congalton RG (1991) A review of assessing the accuracy of classifications of remotely sensed data. *Remote Sens Environ* 37(1):35–46. [https://doi.org/10.1016/0034-4257\(91\)90048-B](https://doi.org/10.1016/0034-4257(91)90048-B)
72. Moisa MB, Gemedo DO (2021) Analysis of urban expansion and land use/land cover changes using geospatial techniques: A case of Addis Ababa City, Ethiopia. *Appl Geomatics* 13(4):853–861. <https://doi.org/10.1007/s12518-021-00397-w>
73. The Tribune (Newspaper) (2022) *Hisar hottest at 48 degrees Celsius as heatwaves intensifies in Haryana.* The Tribune Trust, Chandigarh
74. Mondal A, Guha S, Kundu S (2021) Dynamic status of land surface temperature and spectral indices in Imphal city, India from 1991 to 2021. *Geomatics, Natural Hazards and Risk.* 12(1). 3265–3286. <https://doi.org/10.1080/19475705.2021.2008023>

## Figures

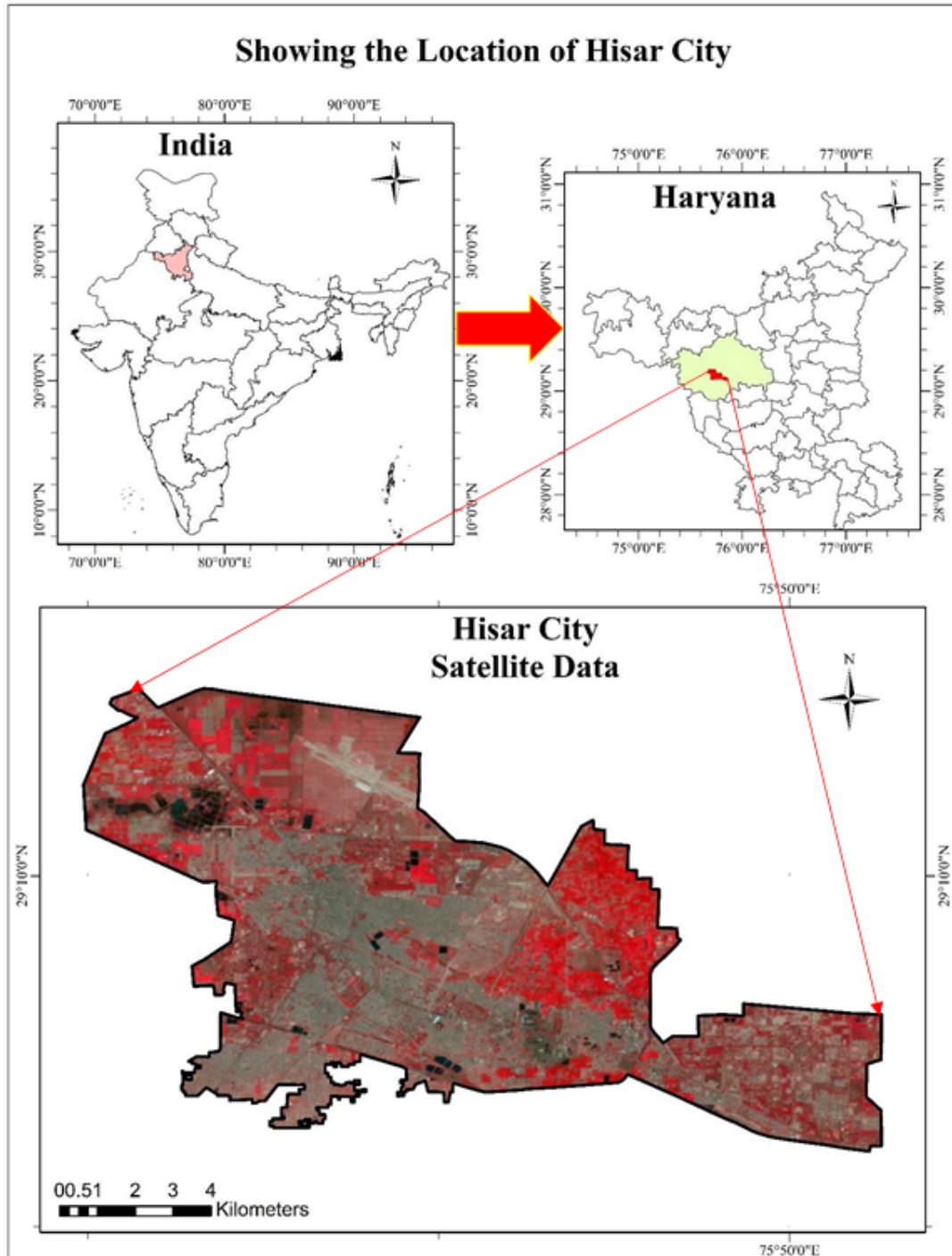


Figure 1

Location map of Hisar city

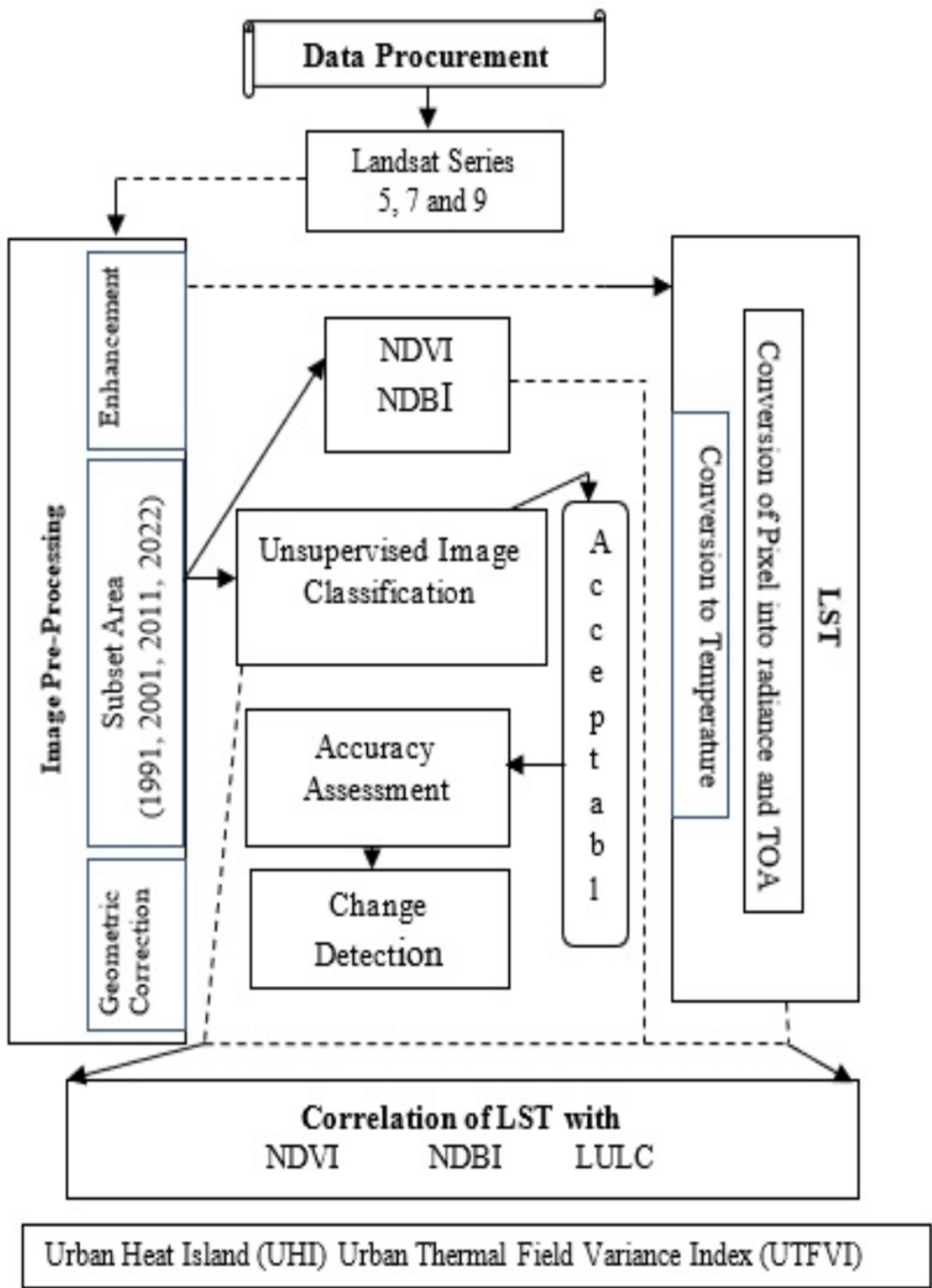
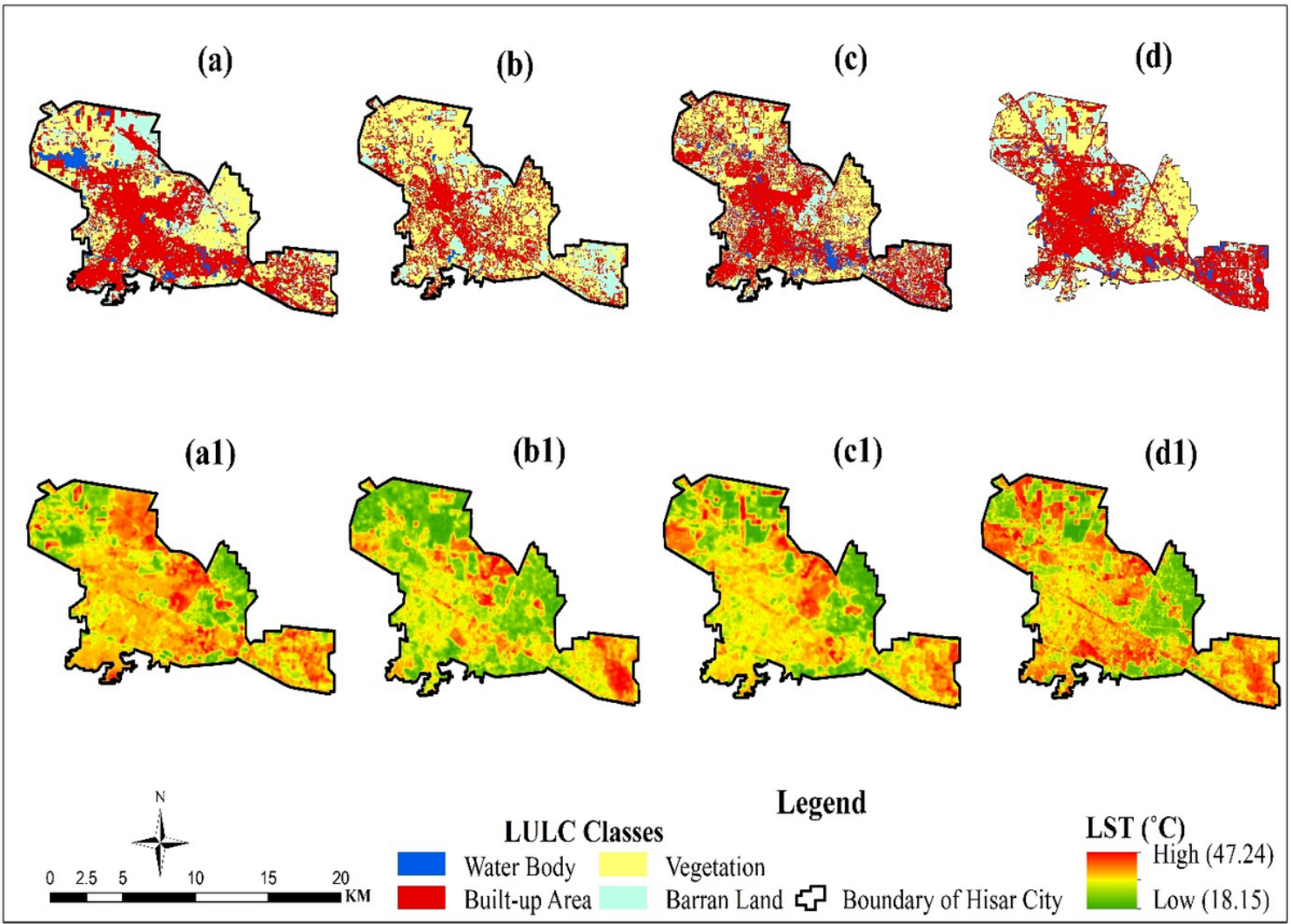


Figure 2

Overall methodology used for research



**Figure 3**

LULC and LST of the Hisar district in 1991, 2001, 2011 and 2022

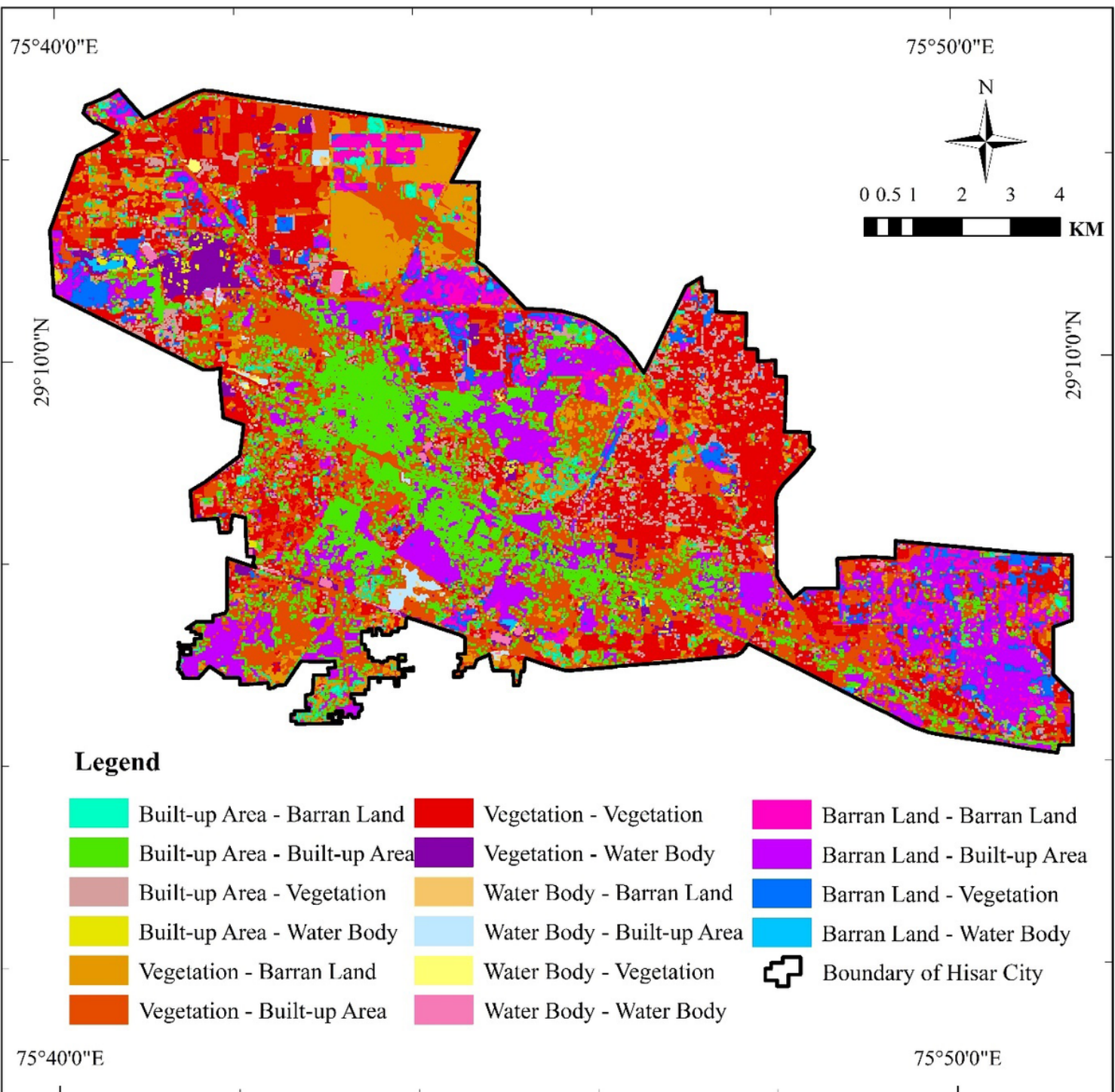


**Figure 4**

Change detection from 1991 to 2022

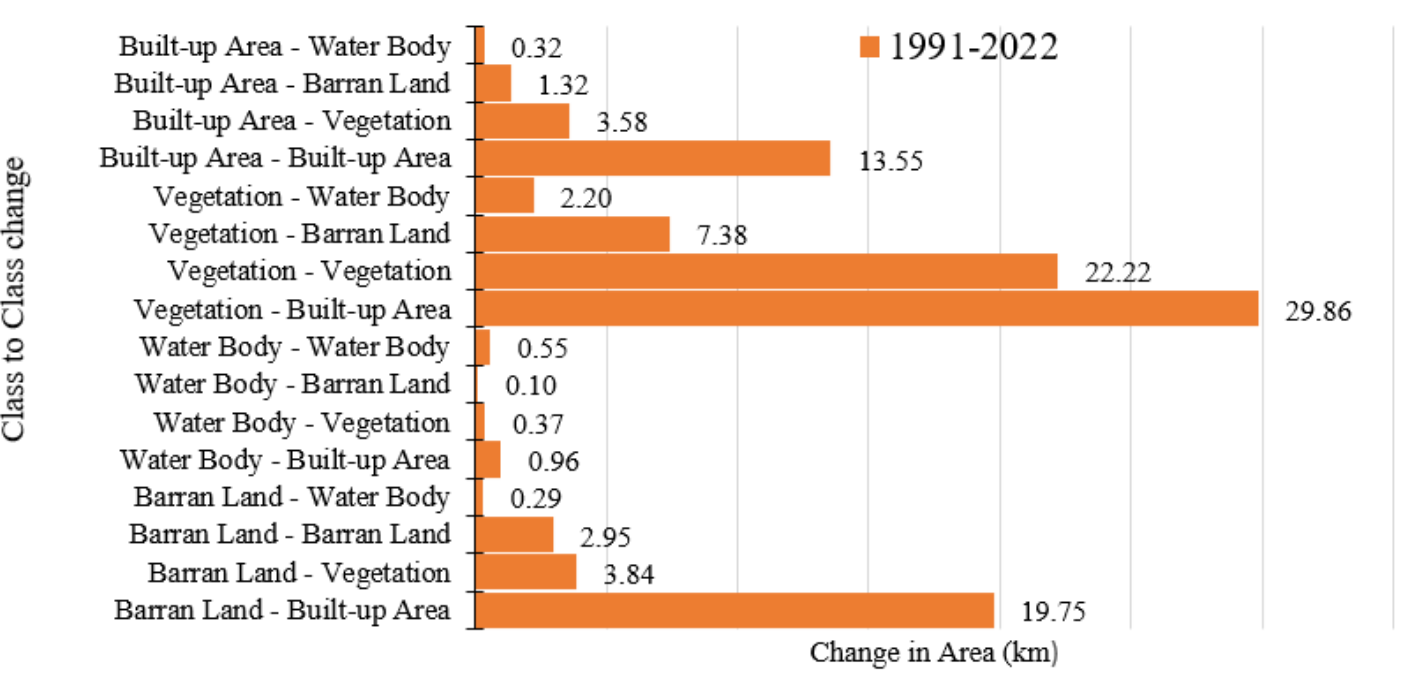


**Figure 5**

Class-to-class changes from 1991 to 2022

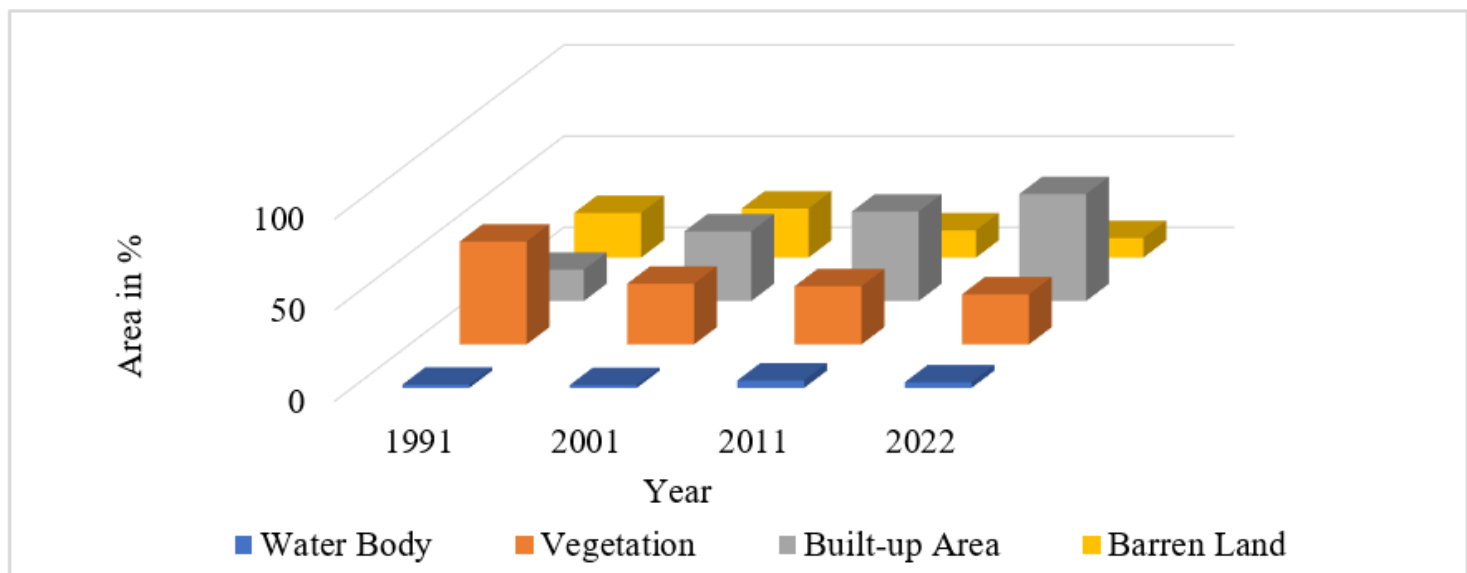


**Figure 6**

Percentage variation in LULC from 1991 to 2022

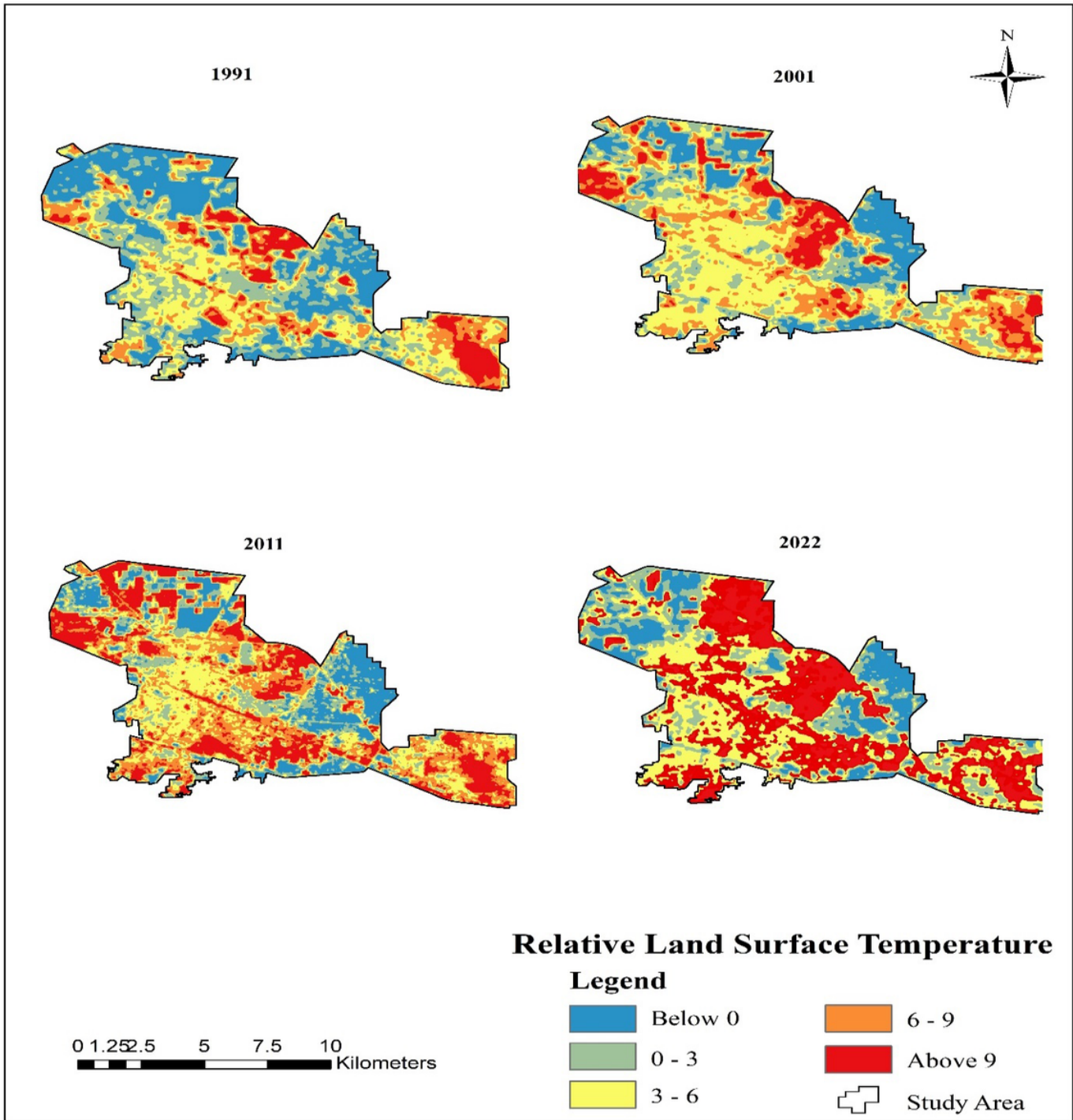
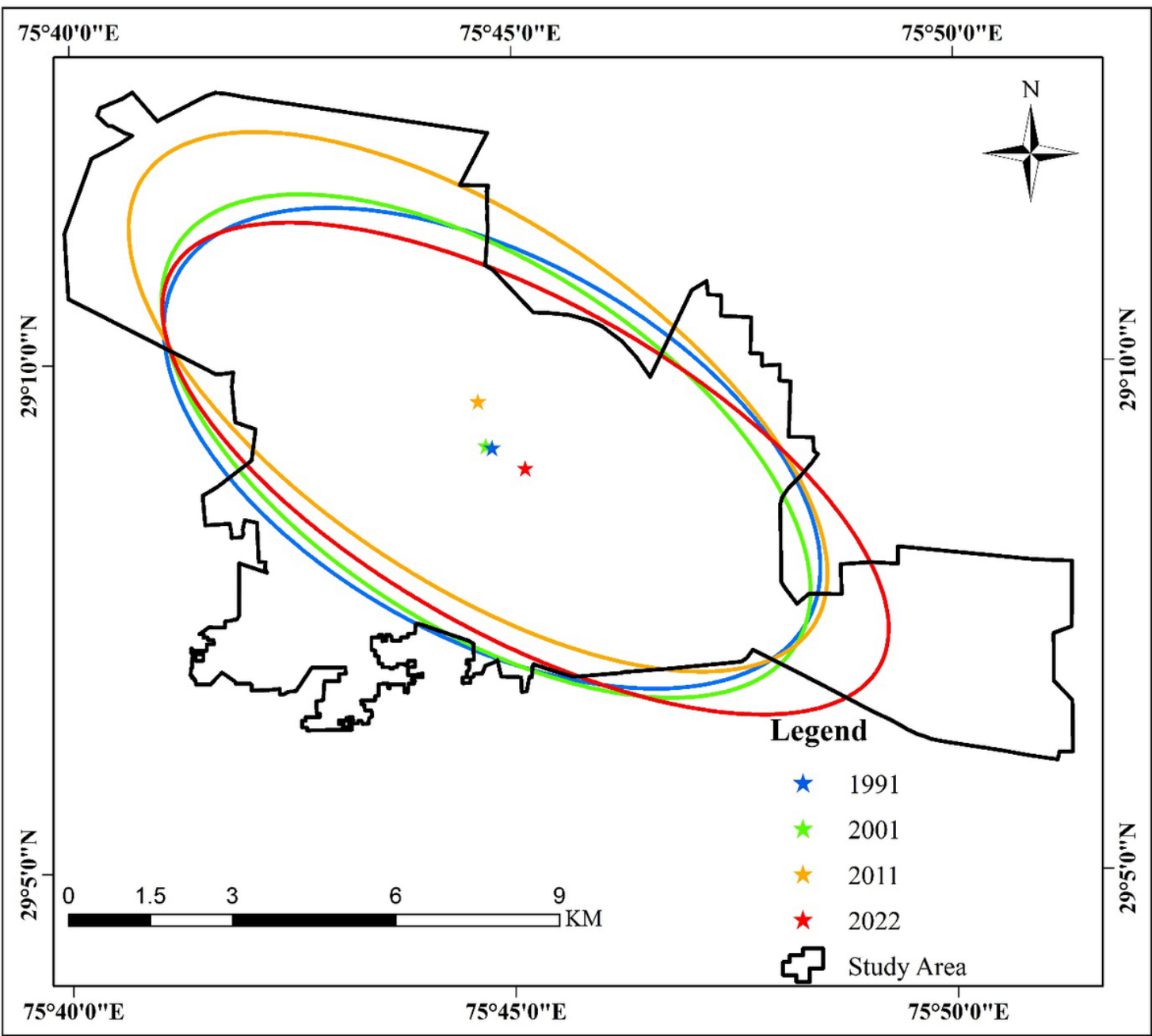


Figure 7

RLST of Hisar



**Figure 8**

SDE zone above 3°C for Hisar

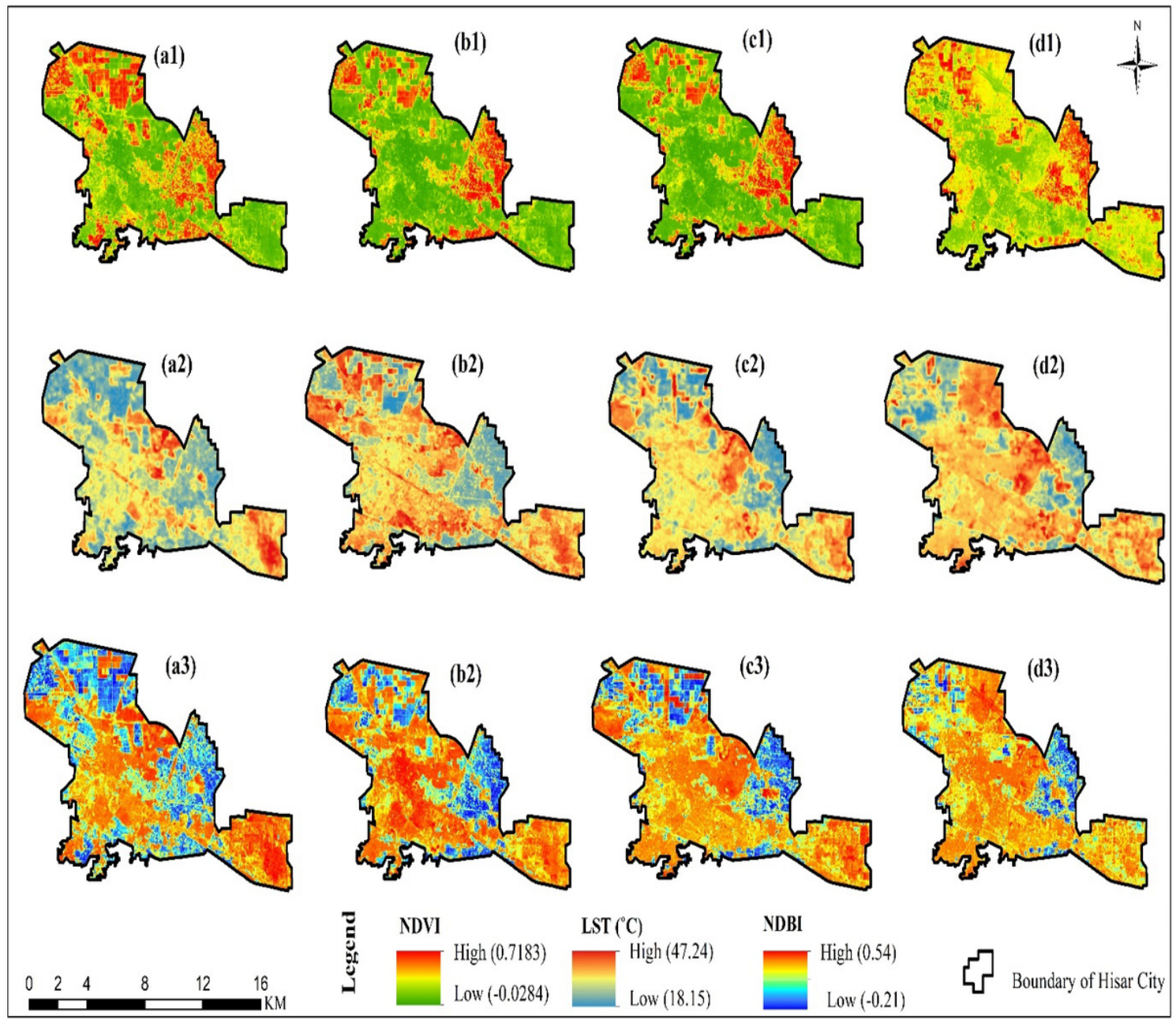


**Figure 9**

(a1, a2, a3; b1, b2, b3; c1, c2, c3; and d1, d2, d3, d4 show the NDVI, LST and NDBI from 1991, 2001, 2011 and 2022 respectively)

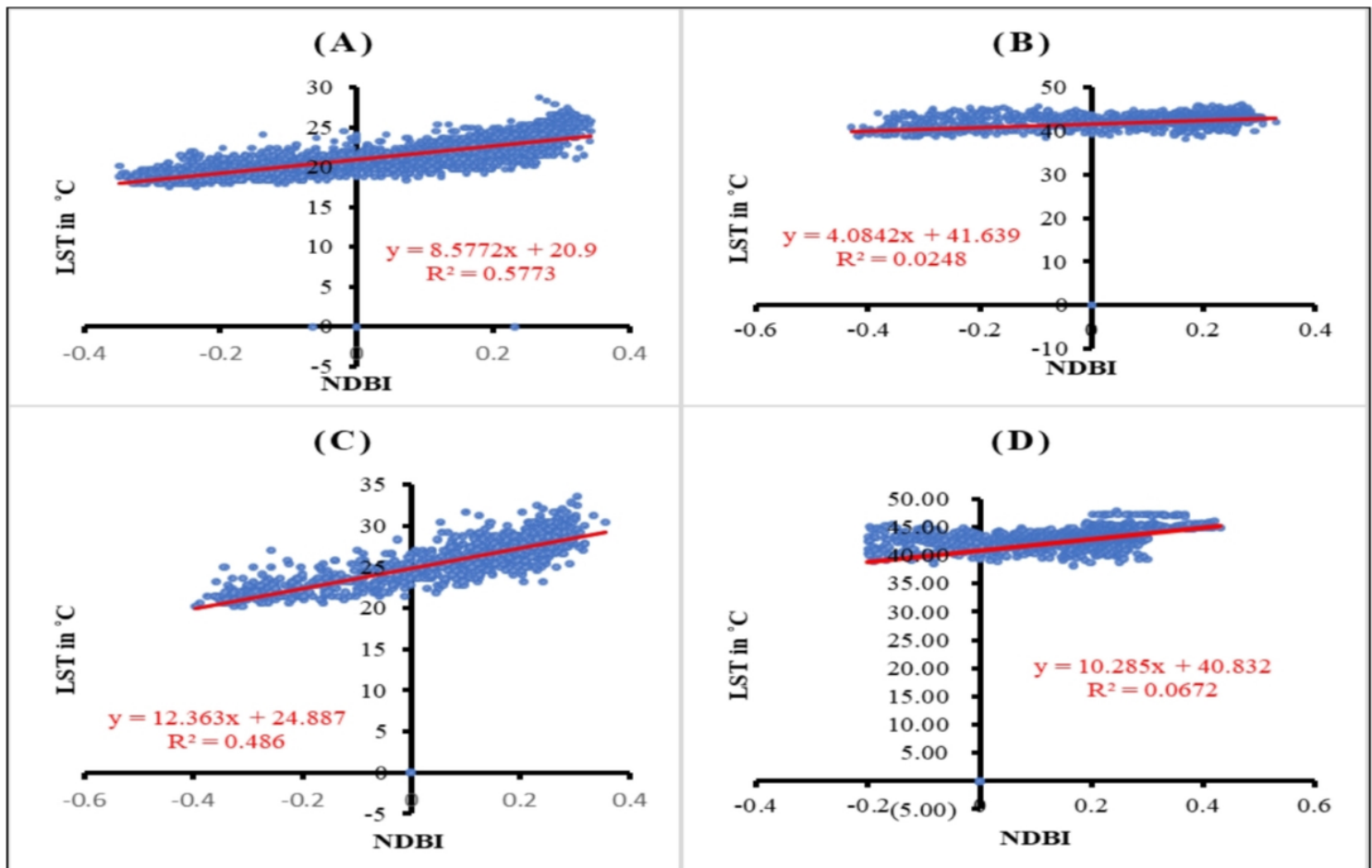


**Figure 10**

Correlations between LST and NDVI in 1991 (A), 2001(B), 2011(C) and 2022 (D)

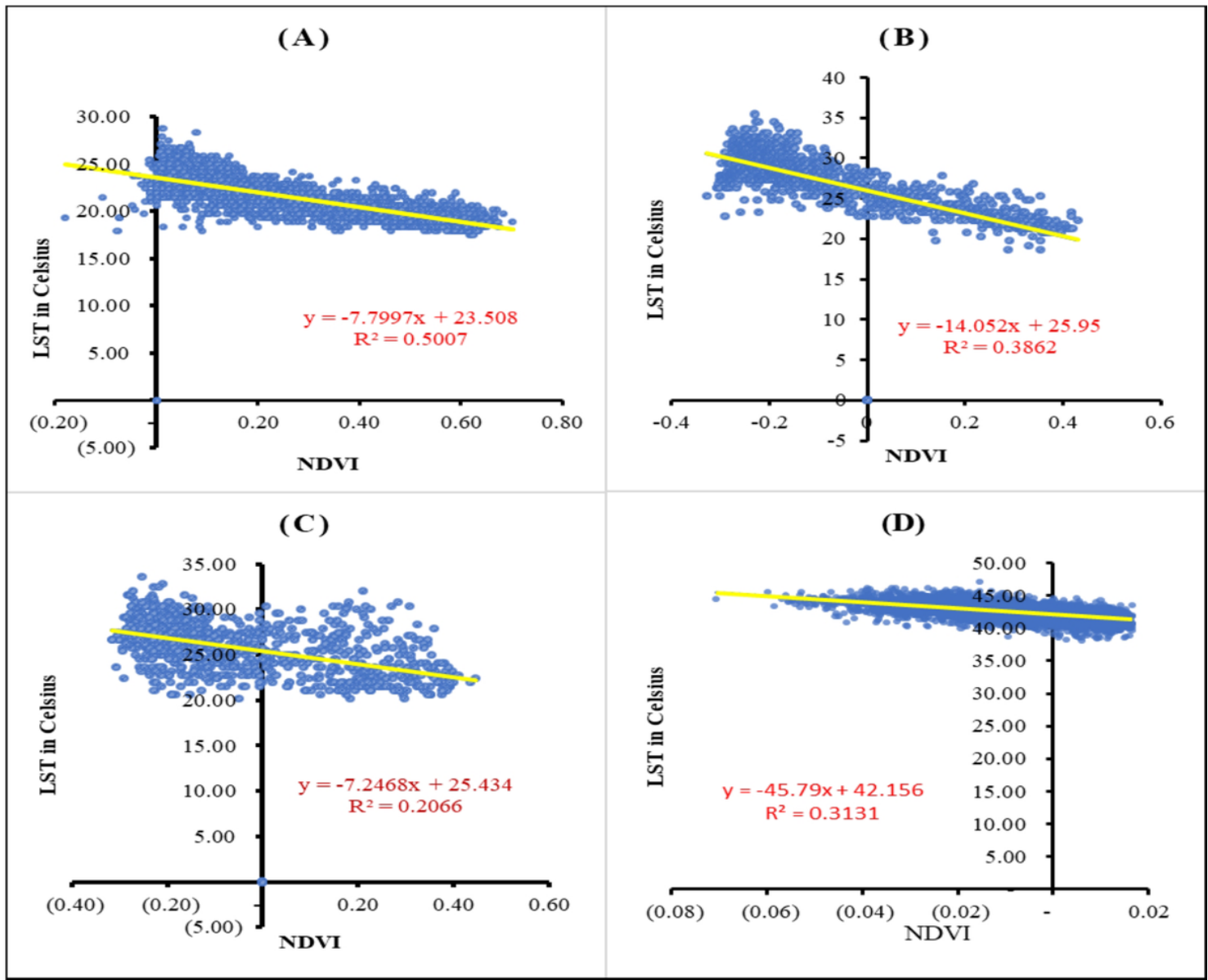


**Figure 11**

Correlations between LST and NDDI in 1991 (A), 2001(B), 2011(C) and- 2022 (D)

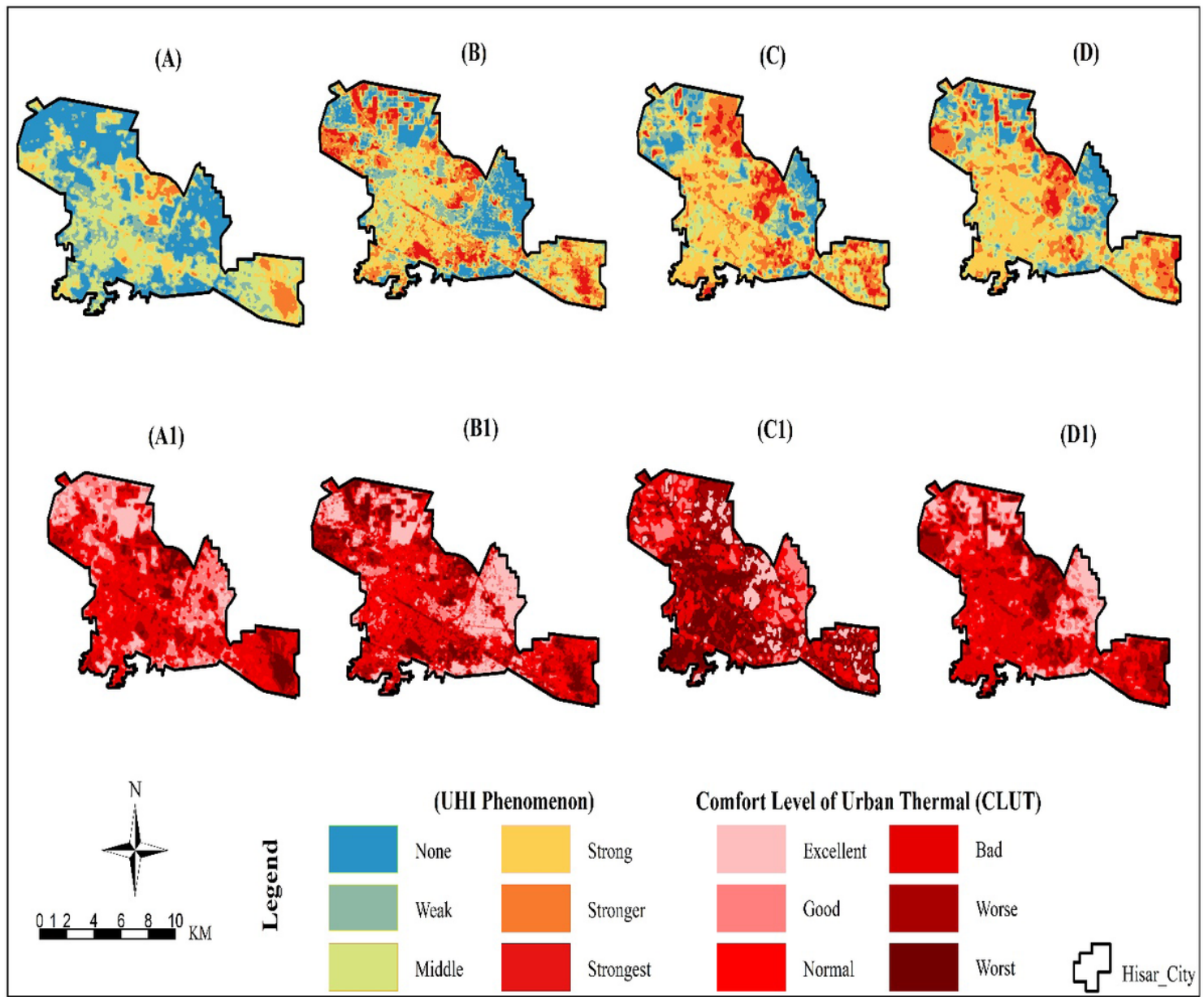


**Figure 12**

UHI and CLUT maps (A, A1; B1, B2; C1, C2; C1,C2 for 1991;2001;2011;2022)